*Neuroscience*

**The Journal of Physiology**

# Relationship between subthalamic nucleus neuronal activity and electrocorticogram is altered in the R6/2 mouse model of Huntington's disease

Joshua W. Callahan and Elizabeth D. Abercrombie

*Center for Molecular and Behavioural Neuroscience, Rutgers University, Newark, NJ 07102, USA*

**Key points**

- Neural synchrony between the subthalamic nucleus (STN) and cortex is critical for proper information processing in basal ganglia circuits.
- Using *in vivo* extracellular recordings in urethane-anaesthetized mice, we demonstrate that single units and local field potentials from the STN exhibit oscillatory entrainment to low-frequency (0.5–4 Hz) rhythms when the cortex is in a synchronized state.
- Here we report novel findings in the R6/2 transgenic mouse model of Huntington's disease (HD) by demonstrating that STN activity is reduced and less phase-locked to cortical low-frequency oscillations.
- The spectral power of low-frequency oscillations in ECoG recordings of R6/2 mice is diminished while the spectral power of higher frequencies is augmented and such altered cortical patterning could lead to decreased synchrony in corticosubthalamic circuits.
- Our data establish that cortical entrainment of STN neural activity is disrupted in R6/2 mice and may be one of the mechanisms contributing to disordered motor control in HD.

**Abstract** Huntington's disease (HD) is an autosomal dominant neurodegenerative disorder in which impairments in the processing of information between the cortex and basal ganglia are fundamental to the onset and progression of the HD phenotype. The corticosubthalamic hyperdirect pathway plays a pivotal role in motor selection and blockade of neuronal activity in the subthalamic nucleus (STN) results in a hyperkinetic movement syndrome, similar to the HD phenotype. The aim of the present study was to examine the relationship between neuronal activity in the STN and cortex in an animal model of HD. We performed *in vivo* extracellular recordings in the STN to measure single-unit activity and local field potentials in the R6/2 transgenic mouse model of HD. These recordings were obtained during epochs of simultaneously acquired electrocorticogram (ECoG) in discrete brain states representative of global cortical network synchronization or desynchronization. Cortically patterned STN neuronal activity was less phase-locked in R6/2 mice, which is likely to result in less efficient coding of cortical inputs by the basal ganglia. In R6/2 mice, the power of the ECoG in lower frequencies (0.5–4 Hz) was diminished while the power expressed in higher frequencies (13–100 Hz) was increased. In addition, the spontaneous activity of STN neurons in R6/2 mice was reduced and neurons exhibited a more irregular firing pattern. Glutamatergic STN neurons provide the major excitatory drive to the output nuclei of the basal ganglia and altered discharge patterns could lead to aberrant basal ganglia output and disordered motor control in HD.

**Abbreviations** CV, coefficient of variation; DA, dopamine; ECoG, electrocorticogram; GPe, globus pallidus external segment; HD, Huntington's disease; ISI, interspike interval; KX, ketamine xylazine; LFO, low-frequency oscillation; LFP, local field potential; M1, primary motor cortex; mHtt, mutant huntingtin; STN, subthalamic nucleus; WT, wild type.

## Introduction

Huntington's disease (HD) is an autosomal dominant neurodegenerative disorder that results in motor, cognitive and psychiatric abnormalities. Evidence indicates that dysfunction across the cerebral cortex is fundamental to the onset and progression of the HD phenotype in humans and animal models of the disease (DiFiglia *et al.* 1997; Sapp *et al.* 1999; Rosas *et al.* 2002; Cepeda *et al.* 2003; Miller *et al.* 2011). The consequences of aberrant cortical drive on the flow of information within cortico-basal ganglia loops is not fully understood and elucidating such alterations could have valuable implications for understanding the precise pathological changes that drive HD disease progression.

The cortex and thalamus provide the main source of glutamatergic inputs into the basal ganglia and project to the striatum and the subthalamic nucleus (STN). The cortex transmits information to the output nuclei of the basal ganglia through the STN with the shortest latency and this 'hyperdirect' circuit is critical in sculpting basal ganglia network activity (Fujimoto & Kita, 1993; Maurice *et al.* 1998; Nambu *et al.* 2000; Magill *et al.* 2001, 2004; Litvak *et al.* 2011). These signals play an important function in movement selection, procedural learning, habit formation and motivational processes (Hamada & DeLong, 1992; Mink, 1996; Baunez & Robbins, 1997; Barnes *et al.* 2005). Blockade of neuronal activity in the STN produces hyperkinetic movement disorders, which mimic chorea, the most common symptom of HD. In animal models, discrete lesions (Whittier & Mettler, 1949; Hamada & DeLong, 1992) or pharmacological inactivation (Carpenter *et al.* 1950) restricted to the STN result in excessive, involuntary movements of the contralateral limbs and thus reflect the importance of control exerted by the STN on motor commands. Presently, it is unknown whether neural activity between the cortex and STN is affected as a function of the expression of the mutant huntingtin protein (mHtt).

The generation of genetic mouse models has helped to elucidate network alterations underlying HD by allowing the direct examination of mechanisms that lead to disease pathogenesis (Raymond *et al.* 2011). In order to examine the effects of mHtt expression on neural processing between the cortex and STN we utilized the R6/2 transgenic mouse model of HD. We tested the hypothesis that synchronous neural activity between the cortex and STN, as previously described in rats (Magill *et al.* 2000, 2001), would be disrupted as a function of mHtt expression. We performed *in vivo* extracellular single-unit recordings in the STN and measured concomitant cortical activity via electrocorticogram (ECoG) in R6/2 mice in order to assess changes in the complex coding of information between these regions in HD.

## Methods

### Animals

Male R6/2 transgenic mice and male wild-type (WT) control mice were studied in the present experiments. All mice were purchased from Jackson Laboratories (Bar Harbor, ME, USA) at 6 weeks of age. Animal orders were timed such that studies for each cohort began approximately 2 weeks after arrival at the animal colony (8–9 weeks of age). The transgenic R6/2 mouse strain (B6CBA-Tg(HDexon1)62Gpb/1 J) was created by Mangiarini and colleagues (1996) and is a fragment model of HD that carries a random insertion of exon 1 of the human Huntingtin (HTT) gene with approximately $160 \pm 5$ polyglutamine repeats (Jackson Laboratories). The resultant expression of the CAG expansion region of the HTT gene produces animals that recapitulate behavioural and neuropathological aspects of human HD with notably early onset and rapid progression of the phenotype (Mangiarini *et al.* 1996). The WT control mouse strain (strain B6CBAF1/J) is the parent strain from which the R6/2 line was developed (Mangiarini *et al.* 1996).

Mice were housed individually in plastic microisolator cages with food and water available *ad libitum*. The mice were maintained under conditions of constant temperature (21°C) and humidity (40%) with a 12 h light–dark cycle (07.00 h on, 19.00 h off). The R6/2 transgenic mice are of generally poor overall health, therefore measures to assist in the maintenance of their vitality were included in the animal husbandry procedures. Moistened food pellets and HydroGel wells (ClearH20, Portland, ME, USA) were placed on the floor of the home cage to facilitate caloric intake and hydration. Nesting pads, composed of compressed cotton fibres, also were provided. All reasonable effort was made in order to minimize animal suffering and to limit the number of animals utilized for these experiments. Animal procedures were conducted in accordance with the National Institutes of Health *Guide for the Care and Use of Laboratory Animals* and were approved by Rutgers University Institutional Animal Care and Use Committee.

### Electrophysiological studies

**Surgical protocol.** Extracellular recording of STN neuronal activity along with simultaneous acquisition of ECoG signal was carried out in the same mice. Anaesthesia was initiated by administration of urethane (1.25 g kg$^{-1}$, I.P.; Sigma-Aldrich Corporation, St Louis, MO, USA). Following the loss of righting reflexes, an appropriate surgical level of anaesthesia was achieved by administration of a solution containing ketamine (80–100 mg kg$^{-1}$, I.P.; Phoenix Pharmaceutical Inc.,

St Joseph, MO, USA) combined with xylazine ($10\ mg\ kg^{-1}$, I.P.; Sigma-Aldrich Corporation). Supplemental doses of ketamine ($30\ mg\ kg^{-1}$, I.P.) plus xylazine ($3\ mg\ kg^{-1}$, I.P.) (KX) were used for the remainder of the experiment as needed (Magill *et al.* 2000; Mallet *et al.* 2008). Sterile saline (0.9% w/v) served as the vehicle for all drug solutions. Throughout the experiment, the effectiveness of this anaesthetic technique was verified by subjective observation of the ECoG signal, the respiration rate, and by testing for the presence of reflex withdrawal to cutaneous paw pinch and corneal stimulation (Whelan & Flecknell, 1992). After the mouse was anaesthetized, local anaesthetic (bupivacaine hydrochloride solution, 0.5%, APP Pharmaceuticals, Schaumburg, IL, USA) was injected beneath the scalp (0.1 ml, S.C.) and the animal was placed into a stereotaxic frame (David Kopf Instruments, Tujunga, CA, USA). With the skull flat, a craniotomy was performed directly above the STN at the following coordinates: AP: −2.1 mm, ML: ± 1.6 mm relative to bregma (Franklin & Paxinos, 2008) and the underlying dura mater was carefully resected. A second craniotomy was performed directly above the ipsilateral primary motor cortex (M1) at the following coordinates: AP: +2.1 mm, ML: ± 2.0 mm relative to bregma (Franklin & Paxinos, 2008). Body temperature was maintained at $37 \pm 0.5°C$ using a heating pad. Lactated Ringer's solution (Fisher Scientific, Suwanee, GA, USA) was administered ($1.0–2.0\ ml\ (30\ g)^{-1}$, S.C.) approximately every 2–3 h to prevent dehydration. All efforts were made to conduct experiments at approximately the same time of day and recordings typically lasted 8–12 h.

The sensitivity of R6/2 mice to anaesthesia has been noted previously (Stern, 2011). Despite extensive empirical work aimed at optimizing the present protocol, the morbidity rate was ~40% in R6/2 mice *versus* 0% for WT mice. For the benefit of other investigators wishing to utilize R6/2 mice under anaesthetized conditions, we report here that preliminary attempts with the anaesthetic agents isoflurane (0.5–3.0% vol. concentration) and Avertin (2, 2, 2-Tribromoethanol; $400\ mg\ kg^{-1}$, I.P.) provided unacceptable outcomes. While neither of these agents was problematic in terms of morbidity, both were associated with effects upon ECoG activity that precluded their use in the examination of the dependent measures of interest in the present studies. Isoflurane induces a burst-suppression pattern in the ECoG that ultimately leads to a continuous isoelectric ECoG signal characteristic of comatose states (Brenner, 1985; Ferron *et al.* 2009). It is interesting to note that we found that Avertin produced ECoG signals consisting of an unusual pattern of low-frequency oscillations entirely lacking in higher frequency components. Thus, we determined that in mice, as in rats (Magill *et al.* 2000; Mallet *et al.* 2008), a combination of urethane followed by supplemental doses

of KX gave the best outcome in terms of preparation viability for the dependent measures of interest.

**STN activity.** Extracellular action potentials generated by single STN neurons and local field potentials (LFP) in STN were recorded from single $10–25\ M\Omega$ glass recording pipettes (tip diameter ~$1.0–2.0\ \mu m$) filled with a 0.5 M NaCl solution containing 2% pontamine sky blue (Sigma-Aldrich Corporation). The electrode was lowered to a point ~$500\ \mu m$ above STN and then was advanced slowly in $1.0–10\ \mu m$ increments using a micropositioner (Model 2660, David Kopf Instruments) until a well-isolated single-unit recording was obtained. Units characteristic of STN neurons recorded in rats such as ~10 Hz firing rates with biphasic waveforms (Magill *et al.* 2000) were encountered 4.0–4.5 mm below dura (see Fig. 1). For all analyses, recordings were used if they were obtained when the electrode track was between AP −1.82 mm to −2.30 mm (relative to bregma). Recordings typically lasted for 2–10 min. The amplified neuronal signals were band-pass filtered between 300 Hz and 20 kHz (Model 1800, A-M Systems Microelectrode Amplifier, Sequim, WA, USA). Amplified LFP signals were band-pass filtered between 0.1 and 20 kHz (A-M Systems Microelectrode Amplifier) and digitized online using a PC and a Micro1401 interface (Cambridge Electronic Design, Cambridge, UK) using Spike2 data acquisition and analysis software (Cambridge Electronic Design). Single-unit activity was sampled at 21 kHz and the LFP
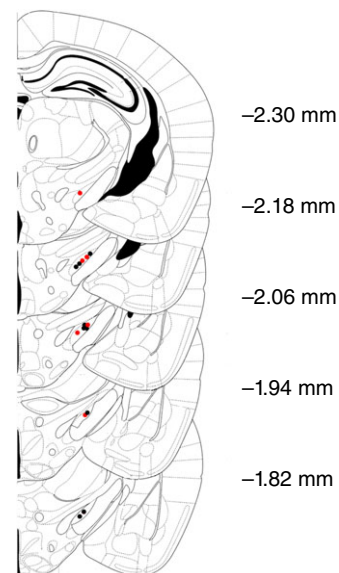


−2.30 mm

−2.18 mm

−2.06 mm

−1.94 mm

−1.82 mm

**Figure 1. Histological confirmation of electrode tracks in the STN**
Schematic coronal diagrams of the mouse brain indicating the location of electrode tracks in the STN (modified from Franklin and Paxinos, 2008) of WT (black) and R6/2 (red) mice. Numbers indicate distance (mm) posterior to bregma.

signal was down-sampled to 500 Hz and low-pass filtered at 100 Hz (Butterworth filter). Data from all recording sessions were visually inspected offline and epochs with breathing or electrical artifacts were discarded.

**ECoG activity.** A bipolar nylon-coated stainless steel electrode (outer diameter 100 $\mu$m, contact separation < 100 $\mu$m) used for ECoG recording was stereotaxically implanted and fixed to the skull using dental cement (Orthodontic Acrylic Resin, Lang Dental Manufacturing Co, Wheeling, IL, USA). A steel screw was fixed into place over the ipsilateral cerebellum to serve as a reference electrode. Raw ECoG was band-pass filtered between 0.1 and 100 Hz (Grass P5 Series Preamplifier; West Warwick, RI, USA). The resulting amplified ECoG signal was sampled at 500 Hz and digitized online with Spike2 data acquisition and analysis software (Cambridge Electronic Design).

The ECoG was monitored continuously throughout all recording sessions that typically lasted from 4 to 8 h. ECoG activity was observed to transition between two distinct states. Epochs of synchronized activity were most prevalent (70% of the time) and were characterized by large amplitude, low-frequency (0.5–4 Hz) oscillations. The desynchronized state (10–20% of the time) consisted of low-voltage activity with remaining time consisting of transitions between these two discrete states. The transition to epochs of desynchronized activity occurred spontaneously and was characterized by sustained high-frequency (15–100 Hz) oscillations. Desynchronized ECoG activity resembles patterns observed during REM sleep or quiet wakefulness (Magill *et al.* 2000, 2001). During these desynchronized epochs, the animal did not show reflexive responses or marked changes in respiration, indicating anaesthesia levels were stable throughout the recording periods.

## Data analysis

**STN single-unit activity.** In order to assess the discharge properties of STN neurons, 30 s epochs of ECoG composed of easily discernable synchronized or desynchronized patterns were identified by visual inspection offline and a portion of the coincident STN spike train consisting of 500 spikes was isolated and further analysed. The mean firing rate (spikes per second) for each STN neuron was calculated. Spike train regularity was determined by calculating the coefficient of variation (CV) of the interspike interval (ISI) distribution (ISI standard deviation/ISI mean). A more detailed analysis of STN spike train patterns was conducted using an automatic burst detection algorithm implemented with custom-derived scripts for use with Spike2 (Cambridge Electronic Design). Specifically, individual ISI histograms were constructed

using a bin size determined by dividing the longest ISI in the spike train into 1000 bins. Bursts were defined as an epoch containing a sequence of two or more spikes beginning with an ISI 40 bins larger than the mode of the ISI distribution and ending with an ISI 80 bins larger than the mode. These parameters were empirically determined to identify events of clustered spiking that occurred in response to the onset of low-frequency oscillatory events in cortex, in contrast to other methods (e.g. Poisson Surprise) that might be used to define 'bursts' of STN neurons or other neurons during desynchronized states. Thus, the burst detection algorithm was only used for the analysis of spike trains recorded during synchronized conditions. For each epoch of STN activity, the number of bursts, percentage of spikes per burst, mean spikes per burst, ISI within bursts, burst duration and inter-burst duration was compared. Lomb periodograms were estimated from the autocorrelograms of spike trains to quantify the significance of any patterns of periodic, oscillatory activity that might be present (Kaneoke & Vitek, 1996). Autocorrelograms were constructed with 20 ms bins and 4 s of lag time for each epoch of STN activity analysed. The frequency bin that contained the highest power within the Lomb periodogram was used as a measure of the dominant oscillatory frequency in a given spike train. We considered oscillations significant if spectral power within these peaks was significantly greater than expected in comparison with independent Gaussian random variables ($P < 0.05$). Those neurons that displayed significant peaks in the periodogram spectra between 0.5–4 Hz were classified as exhibiting significant low-frequency oscillations and termed LFO in the subsequent text.

**Cortical ECoG activity.** In order to assess the spectral composition of ECoG we performed Fast Fourier transform (FFT) analysis. Estimates of the spectral power density were extracted via Welch's periodogram method using a Hanning window with 50% overlap and a resolution frequency of 0.242 Hz. Estimates were summed within the following frequency bins to obtain the power densities of low-frequency and higher frequency band-widths: 0.5–4 Hz, 4–7 Hz, 7–13 Hz, 13–30 Hz and 30–100 Hz.

**Coherence between STN activity and ECoG.** Coherence measures the amount of linear correlation between two time series as a function of frequency and is an absolute value that varies between 0, no systematic phase relationship between two signals, and 1, indicating a perfect phase relationship (i.e. phase-locked). The coherence between STN activity (unit firing or LFP) with coincident ECoG was calculated using the multitaper method implemented in the Chronux 2.0 data analysis

toolbox (Bokil *et al.* 2010) for Matlab (MathWorks). Coherence spectra were estimated for the frequency range from 0.5 to 100 Hz. We extracted the peak coherence value for statistical comparison.

**Histology.** To identify the location of recorded sites, at the end of each experiment the electrode placement of the last recorded neuron was marked with an iontophoretic deposit of Pontamine Sky Blue (15–20 min, −20 μA, constant current injection). Upon completion of each experiment, animals were administered a lethal dose of sodium pentobarbital and were perfused intracardially with 0.9% saline followed by 10% formaldehyde. Brains were extracted and post-fixed in fresh fixative overnight at 4°C and transferred to 30% sucrose in phosphate buffer solution at 4°C for cryoprotection. Coronal sections of 60 μm thickness were obtained and stained with Neutral Red (Sigma-Aldrich Corporation) to verify the recording site in the STN (Fig. 1).

**Statistical analysis.** All data are presented as means ± SEM. Data were analysed with a Student's *t* test for unpaired comparisons and by using a Mann–Whitney U test for non-parametric procedures. Between-group differences for paired comparisons were assessed using two-way ANOVA. When appropriate, two-way ANOVA determinations were followed by Bonferroni's *post hoc* test. For the analysis of within-group effects for paired comparisons, one-way ANOVA was used coupled to Bonferroni's *post hoc* test. Between-group differences for three comparisons were assessed using one-way ANOVA coupled to Bonferroni's *post hoc* test when appropriate. For the analysis of group differences for three comparisons with non-normal distributions, a Kruskal–Wallis test was used together with Dunn's *post hoc* test. Differences were considered statistically significant when $P < 0.05$.

## Results

### Experimental overview

A total of nine WT ($n = 65$ STN neurons) and six R6/2 mice ($n = 45$ STN neurons) were included in the present experiments. Single-unit recordings of STN activity were acquired during epochs of synchronized or desynchronized ECoG states. The proportion of time within synchronized and desynchronized ECoG conditions did not differ between genotypes. In some cases, recording conditions permitted STN activity to be acquired from a single neuron during both ECoG states in WT ($n = 7$ neurons) and R6/2 ($n = 8$ neurons) mice. For the WT group, STN neurons recorded during synchronized ECoG epochs exhibited low-frequency

oscillations (LFO) that were phase-locked to coincident slow ECoG oscillations. For the R6/2 group, ~20% of STN neurons recorded during synchronized ECoG states did not exhibit significant periodicity in their spike trains according to the Lomb analysis and are termed *tonic* in the subsequent text. Data collected from tonic neurons were therefore analysed separately from LFO neurons.

### Firing properties of STN neurons are dependent on ECoG state

Figure 2 shows a representative example collected from WT mice depicting the patterns of activity of STN units during synchronized and desynchronized ECoG epochs. STN neurons preferentially fire bursts of action potentials that are phase-locked to cortical up states during synchronized ECoG epochs. In contrast, STN neurons fire with more tonic regularity during desynchronized ECoG epochs. The firing patterns of STN neurons that we report in WT mice are consistent with that reported previously in rats (Magill *et al.* 2000, 2001).

### STN spike train activity in the synchronized ECoG state in R6/2 mice

Figure 3*A* shows a representative example depicting the firing properties of tonic STN neurons recorded from R6/2 mice during synchronized ECoG epochs. In R6/2 mice, tonic STN neurons discharged with significantly reduced spike rates relative to LFO STN neurons ($H = 8.64$, d.f. = 2, $P < 0.05$; Table 1). Moreover, the CV of tonic STN neurons was significantly less than that of LFO STN neurons recorded in both R6/2 and WT mice ($H = 12.26$, d.f. = 2, $P < 0.01$; Table 1). The number of burst events in LFO STN neurons recorded from R6/2 mice was significantly less than recorded in LFO STN neurons from WT mice ($63.95 \pm 4.07$; $U(58) = 299.0$, $P < 0.05$; Table 1). In addition, the duration between burst events was significantly shorter in LFO STN neurons recorded from R6/2 mice relative to that recorded in LFO STN neurons from WT mice ($U(58) = 167.0$, $P < 0.01$; Table 1). There was no significant difference in the number of action potentials per burst in LFO STN neurons recorded from R6/2 mice ($8.03 \pm 0.79$) in comparison to that recorded in LFO STN neurons from WT mice ($8.18 \pm 0.55$; $U(58) = 301.0$, $P < 0.05$; Table 1). There was no significant difference between genotypes in the percentage of spikes within bursts ($t(58) = 0.02$, $P = 0.49$), the ISI of spikes within bursts ($U(58) = 362.5$, $P = 0.20$) or the burst duration ($t(58) = 0.01$, $P = 0.49$) in LFO STN neurons. In addition, there was no significant difference between genotypes in the peak oscillating frequency of the spike train in LFO STN neurons ($U(58) = 343.5$, $P = 0.13$; Table 1).

## STN spike train activity in the desynchronized ECoG state in R6/2 mice

Figure 3*B* shows a representative example depicting the firing properties of STN neurons recorded from R6/2 mice during desynchronized ECoG epochs. Neurons recorded from the STN in R6/2 mice discharged with significantly slower firing rates compared to STN units recorded in WT mice ($U (56) = 197.0$, $P < 0.01$; Table 1). In addition, the CV of the ISI distribution was significantly larger in STN neurons recorded from R6/2 mice in comparison to

STN neurons recorded from WT mice ($U (56) = 240.0$, $P < 0.01$; Table 1).

## Spectral composition of ECoG in the synchronized state

The dominant frequency of the ECoG was significantly higher during recording epochs in both LFO ($1.78 \pm 0.18$ Hz) and tonic STN neurons ($1.68 \pm 0.05$ Hz) in R6/2 mice in comparison to those collected from LFO STN neurons in WT mice ($1.42 \pm 0.04$ Hz; $F(2, 63) = 8.63$,
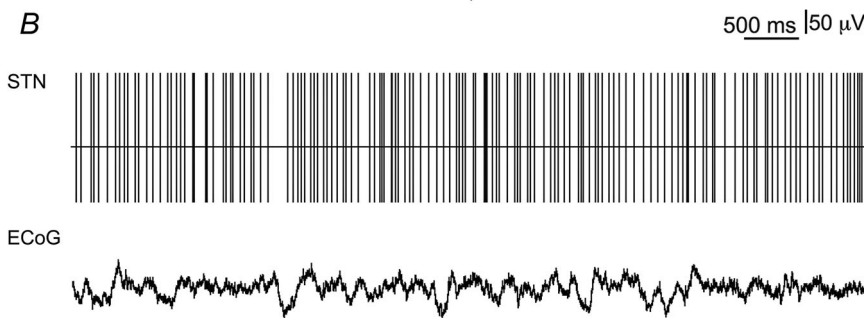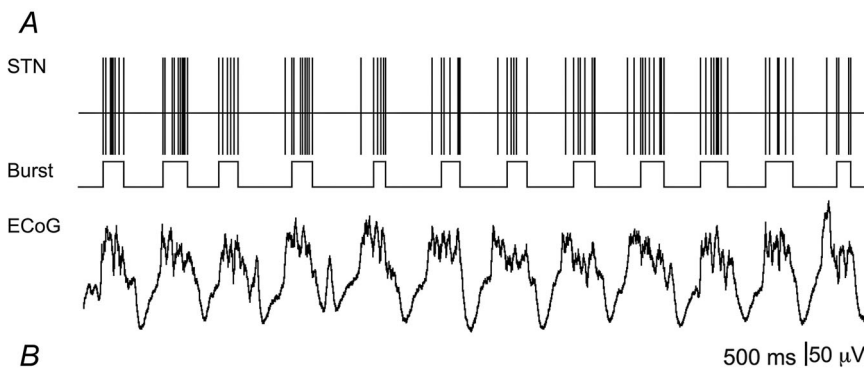


**Figure 2. Representative neuronal activity in the STN and concomitant ECoG collected from WT mice**
In this and other similar figures, the spike train is represented by the output of the spike detection channel of the CED software and exhibits spike timing. *A*, spike train of LFO STN neuron (firing rate = 8.34 Hz; CV = 1.36; Lomb frequency = 1.45 Hz) recorded during synchronized ECoG epoch. Middle trace, rhythmic burst events are phase-locked to cortical up states. *B*, spike train of STN neuron (firing rate = 17.23 Hz; CV = 0.59) recorded during desynchronized ECoG epoch.
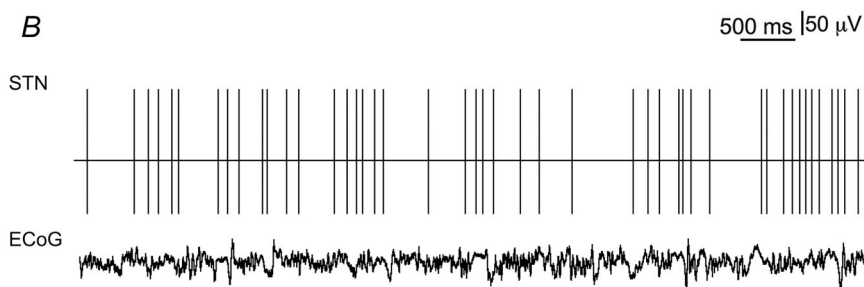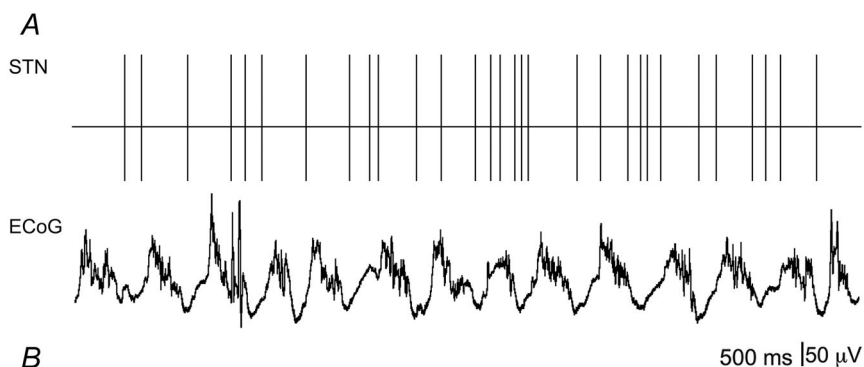


**Figure 3. Representative neuronal activity in the STN and concomitant ECoG collected from R6/2 mice**
*A*, spike train of tonic STN neuron (firing rate = 4.31 Hz; CV = 0.56) recorded during synchronized ECoG epoch. *B*, spike train of STN neuron (firing rate = 7.35 Hz; CV = 1.16) recorded during desynchronized ECoG epoch.

**Table 1. Firing properties of STN neurons**

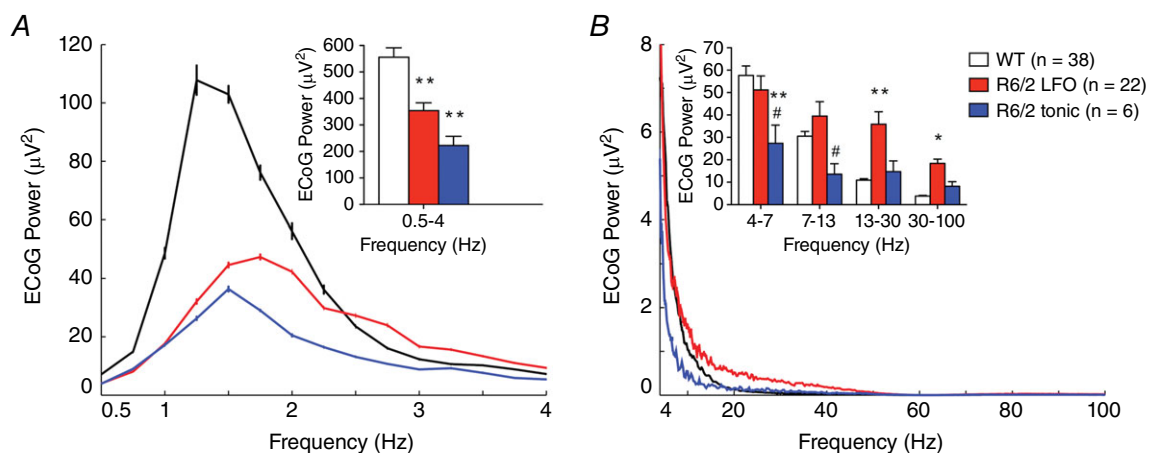| | Synchronized epochs | | | Desynchronized epochs | |
|---|---|---|---|---|---|
| | WT | R6/2 LFO | R6/2 tonic | WT | R6/2 |
| Number of cells | 39 | 28 | 6 | 33 | 25 |
| Firing rate (Hz) | $12.52 \pm 1.23$ | $15.13 \pm 0.78$ | $8.97 \pm 2.26^{\#}$ | $17.23 \pm 1.40$ | $10.71 \pm 0.97^{**}$ |
| Coefficient of variation | $1.40 \pm 0.08$ | $1.36 \pm 0.05$ | $0.69 \pm 0.12^{**,\#\#}$ | $0.59 \pm 0.03$ | $0.96 \pm 0.12^{**}$ |
| Number of bursts | $63.95 \pm 4.07$ | $54.18 \pm 2.92^{*}$ | — | — | — |
| Interburst duration (ms) | $601.10 \pm 29.97$ | $446.20 \pm 19.38^{**}$ | — | — | — |
| Lomb frequency (Hz) | $1.37 \pm 0.05$ | $1.48 \pm 0.12$ | — | — | — |

All data are means $\pm$ SEM. *Significantly different from WT, $P < 0.05$; **significantly different from WT, $P < 0.01$; #significantly different from R6/2 LFO, $P < 0.05$; ##significantly different from R6/2 LFO, $P < 0.01$.

$P < 0.01$). The total power of the ECoG within the lowest frequency bandwidth (0.5–4 Hz) was significantly diminished during recording epochs in both LFO and tonic STN neurons in R6/2 mice in comparison to those collected from LFO STN neurons in WT mice ($H = 18.52$, d.f. $= 2$, $P < 0.01$; Fig. 4$A$). The total power of the ECoG in higher frequencies (4–100 Hz) was significantly skewed as a function of genotype ($F (2, 63) = 5.13$, $P < 0.01$) and bandwidth ($F (3, 63) = 62.20$, $P < 0.01$) and there was a significant genotype × bandwidth interaction ($F (6, 63) = 12.20$, $P < 0.01$). Planned comparisons indicated that the power within 13–30 Hz and 30–100 Hz was greater during recording epochs in LFO STN neurons from R6/2 mice relative to those collected in LFO STN neurons from WT mice (Fig. 4$B$). Furthermore, the power within 4–7 Hz was less during recording epochs in tonic STN neurons in R6/2 mice in comparison to those collected from LFO STN neurons in WT mice (Fig. 4$B$). In addition, the power

within 4–7 Hz and 7–13 Hz was lower during recording epochs in tonic STN neurons relative to those collected from LFO STN neurons recorded in R6/2 mice (Fig. 4$B$).

## Coherence between STN activity and ECoG in the synchronized state

The coherence between STN unit spiking and ECoG, specifically within the lowest frequency bandwidth (0.5–4 Hz), was significantly reduced in both LFO ($0.63 \pm 0.04$) and tonic STN neurons ($0.56 \pm 0.06$) in R6/2 mice compared to those collected in WT mice ($0.81 \pm 0.02$; $H = 19.77$, d.f. $= 2$, $P < 0.01$; Fig. 5$B$). Likewise, the coherence between STN LFP activity and ECoG, specifically within the lowest frequency bandwidth, was significantly reduced in R6/2 mice ($0.69 \pm 0.2$) in comparison to WT mice ($0.83 \pm 0.02$; $t (7) = 4.91$, $P < 0.01$, $n = 6$ WT, $n = 3$ R6/2; Fig. 5$C$).



**Figure 4. Spectral composition of ECoG in the synchronized state**
Power spectrum of the ECoG during synchronized epochs concomitant to the recording of WT STN neurons (black), R6/2 LFO STN neurons (red), and R6/2 tonic STN neurons (blue). *A*, total power spectral density of ECoG within low-frequency components. *B*, total power spectral density of ECoG within high-frequency components. All data are means $\pm$ SEM. *Significantly different from WT, $P < 0.05$; **significantly different from WT, $P < 0.01$; #significantly different from R6/2 LFO, $P < 0.05$.

## Spectral composition of ECoG in the desynchronized state

The total power of the ECoG within the lowest frequency bandwidth (0.5–4 Hz) was significantly attenuated during recording epochs in STN neurons in R6/2 mice in comparison those collected in WT mice ($t_{(56)} = 5.18$,
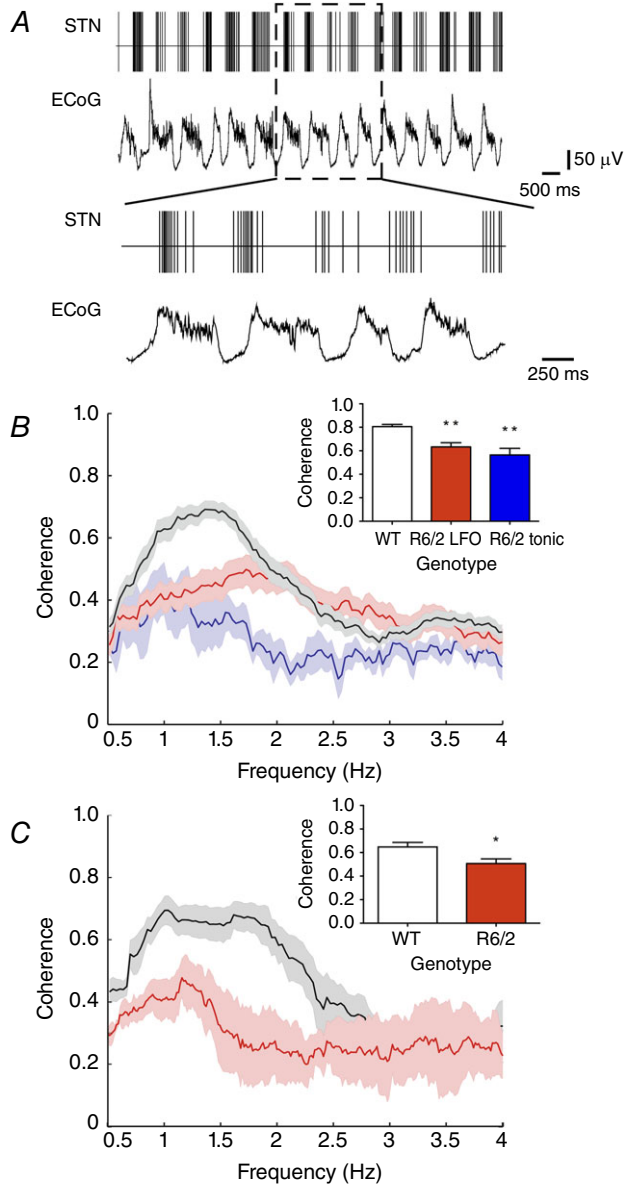
$P < 0.01$; Fig. 6). The total power of the ECoG in higher frequencies (4–100 Hz) was significantly altered as a function of genotype ($F_{(1, 56)} = 8.49$, $P < 0.01$) and bandwidth ($F_{(3, 56)} = 14.12$, $P < 0.01$) and there was a significant genotype × bandwidth interaction ($F_{(3, 56)} = 33.14$, $P < 0.01$). Planned comparisons indicated that the power within 13–30 Hz and 30–100 Hz was higher during recording epochs in STN neurons in R6/2 mice in comparison to those collected from STN neurons in WT mice (Fig. 6). In addition, the power within 4–7 Hz was diminished during recording epochs in STN neurons in R6/2 mice in comparison to those collected from STN neurons in WT mice (Fig. 6).

## Coherence between STN activity and ECoG in the desynchronized state

We found no significant difference in the coherence between STN unit spiking and ECoG within the lowest frequency bandwidth (0.5–4 Hz) in R6/2 mice ($0.32 \pm 0.02$) as compared to WT mice ($0.31 \pm 0.01$; $U_{(56)} = 412.0$, $P = 0.50$).

## Discussion

The present study was undertaken to investigate how the flow of information between the cerebral cortex and the STN is altered as a function of the expression of the mHtt protein in the R6/2 transgenic mouse model of HD. Our results demonstrate that cortically patterned STN neuronal discharge is markedly less synchronized in R6/2 mice.
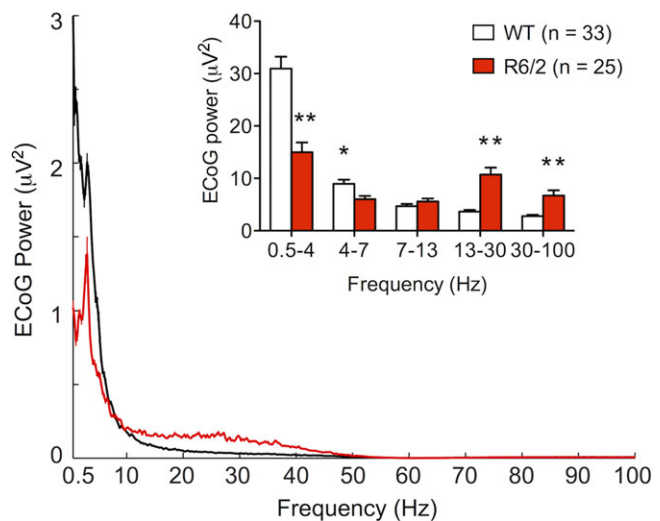


**Figure 5. Oscillatory entrainment of STN neuronal activity during synchronized ECoG epochs**
*A*, spike train of R6/2 LFO STN neuron (firing rate = 17.68 Hz; CV = 1.82) recorded during synchronized ECoG epoch. Bottom trace, magnified demonstration of reduced phase synchronization of STN neuronal spike discharge to coincident ECoG LFO. *B*, coherence between STN neuronal spike discharge and coincident ECoG activity as a function of frequency. *C*, coherence between STN LFP activity and coincident ECoG activity as a function of frequency. All data are means ± SEM. **Significantly different from WT, $P < 0.01$.



**Figure 6. Spectral composition of ECoG in the desynchronized state**
ECoG spectral power acquired in desynchronized epochs concomitant to the recording of WT (black) and R6/2 (red) STN neurons. Inset, total power spectral density of ECoG. All data are means ± SEM. *Significantly different from WT, $P < 0.05$; **significantly different from WT, $P < 0.01$.

In addition, the spontaneous activity of STN neurons in the absence of synchronized cortical input is diminished in R6/2 mice.

Under urethane–KX anaesthesia, global cortical activity alternates between periods of synchronized and desynchronized states, which have differential effects on shaping the neuronal activity in the STN (Magill *et al.* 2000, 2001; Mallet *et al.* 2008). During synchronized ECoG states, large ensembles of cortical neurons oscillate in synchrony between depolarized up states and quiescent hyperpolarized down states (Steriade, 2001). This pattern of rhythmic activity is expressed in the ECoG as recurring large amplitude, low-frequency (∼1 Hz) oscillations (Steriade *et al.* 1993; Amzica & Steriade, 1998). Such rhythmic cortical patterning has a powerful synchronizing effect on STN activity and leads to the entrainment of neuronal firing in the STN (Magill *et al.* 2000, 2001; Bevan *et al.* 2002). Similar to findings reported in urethane-anaesthetized rats during synchronized ECoG conditions (Magill *et al.* 2000, 2001), we observed significant LFO discharge characteristics in the spike trains of all STN neurons recorded from WT mice. STN unit and LFP activity were phase-locked to cortical up states and highly synchronized to concomitant LFO cortical rhythms. Thus, the urethane–KX-anaesthetized animal enables stereotyped control over ECoG organization and serves as an effective model for assessing the functional connectivity between the cortex and the STN (Magill *et al.* 2000, 2001; Mallet *et al.* 2008).

During synchronized ECoG states, powerful cortical LFO transmission is propagated to the STN. In contrast to the homogeneous patterns of phase-locked spiking that we observed in WT mice, strikingly, ∼20% of STN neurons recorded from R6/2 mice failed to discharge with LFO patterns. The firing rate and pattern of activity in these tonic STN neurons resembled that observed in the desynchronized ECoG state, when cortical entrainment is less prominent and spiking is more autonomous (Bevan *et al.* 2002). While the remainder of neurons (∼80%) recorded from the STN population in R6/2 mice fired with the expected LFO discharge, there was a marked change in the nature of the relationship between oscillatory activity in the STN and the cortex. In WT mice, STN neurons preferentially fire bursts of action potentials that are phase-locked to cortical up states; however, R6/2 LFO STN neurons fired with significantly fewer bursts and the degree of phase-locking between STN spiking and concomitant cortical LFO activity was significantly reduced. Loss of entrainment of STN activity was also seen at the network level as the coherence between the STN LFP and cortical LFO activity was attenuated. Thus, these results suggest that cortical entrainment of STN neuronal activity is significantly disrupted in R6/2 mice.

The overall spectral composition of cortical activity during synchronized states was altered in R6/2 mice. Specifically, the density of power of low-frequency oscillations in the ECoG was reduced and the power expressed in higher frequencies was increased in R6/2 mice. During synchronized states, reductions in the spectral power of the ECoG at low frequencies suggests that the excitatory cortical drive to the STN is reduced, as an ensemble of neurons are more effective in recruiting their postsynaptic targets if they discharge in synchrony rather than if they fire asynchronously. During synchronized conditions, high-voltage cortical LFO activity is generated by cortical pyramidal neurons (Steriade *et al.* 2001; Hughes & Crunelli, 2013; Kuki *et al.* 2013). While neuronal loss in the cortex has not been reported in 9-week-old R6/2 mice, reductions in cortical volume are apparent. Cortical volume reduction has been linked to morphological alterations of pyramidal neurons, which include reductions in somatic size, decrease density of dendrites and loss of dendritic spines (Turmaine *et al.* 2000; Klapstein *et al.* 2001; Laforet *et al.* 2001; Stack *et al.* 2005). These characteristics are similar to dendritic changes reported in pyramidal cells of HD postmortem brains (Sotrel *et al.* 1993; Vonsattel & DiFiglia, 1998). Network summations of oscillations are only apparent when neurons oscillate coherently and such structural alterations could lead to reductions in the strength of connectivity and diminished correlated activity between cells. In accordance, correlated firing patterns are reduced in cortical neurons recorded from R6/2 mice during awake, behaving conditions (Walker *et al.* 2008). Reduced cortical plasticity has also been shown in both R6/2 mice and human HD patients and could contribute to the diminished capacity to generate high-voltage LFO activity in the cortex (Kung *et al.* 2007; Crupi *et al.* 2008; Dallerac *et al.* 2011).

In contrast to reductions in power of low-frequency oscillations in R6/2 mice, oscillations in higher frequency ranges were increased. A shift in spectral density towards higher frequencies has also been demonstrated in R6/2 mice during awake, behaving conditions and confirms that the patterns we report are not merely an artifact of anaesthesia (Hong *et al.* 2012; Fisher *et al.* 2013; Kantor *et al.* 2013). Chronic depletion of dopamine (DA) can dramatically increase the power of cortical oscillations in higher frequency ranges, specifically in the 13–30 Hz range (Brown, 2003). This shift is likely to be a consequence of plasticity induced by long-term progressive dopamine depletion (Nambu *et al.* 2002; Brown, 2003). In accordance, deficits in DA release and storage have been reported as early as 6 weeks of age in R6/2 mice (Hickey *et al.* 2002; Johnson *et al.* 2006; Callahan & Abercrombie, 2011; Mochel *et al.* 2011). Such influences could contribute to the increased expression of higher frequency oscillations in R6/2 mice and lead to recruitment errors in the cortical entrainment of STN neuronal activity. In addition, the STN receives afferents

from other regions that can modulate STN neuronal activity and we cannot rule out these influences. These include projections from the parafasicular nucleus of the thalamus (Bevan *et al.* 1995), dorsal raphe nuclei (Lavoie & Parent, 1990), substantia nigra pars compacta (Hassani *et al.* 1997), and the pedunculopontine nucleus (Jackson & Crossman, 1983).

While investigating neural patterns of activity in the STN during synchronized ECoG states is invaluable for determining the fidelity of transmission in corticosubthalamic pathways, activity measured during desynchronized conditions is advantageous in that it more closely resembles activity patterns seen during wakefulness (Steriade, 2001). This is especially important in view of the fact that chorea manifests during waking and is absent during states resembling synchronized ECoG conditions, such as sleep (Morton, 2013). In contrast to periods of cortical synchronization, epochs of desynchronization are associated with a persistently depolarized state in which low-frequency oscillations are attenuated and replaced by higher frequency oscillations in the ECoG (Steriade, 2001). Hence, desynchronization rapidly restructures the spectral composition of cortical activity and as a result the powerful synchronizing drive of the cortex on the STN is diminished. During desynchronized ECoG states, STN neurons discharge with higher firing rates and tonic regularity and this autonomous activity is largely a result of intrinsic mechanisms, such as persistent sodium currents (Bevan & Wilson, 1999).

During desynchronized ECoG epochs, we found significant reductions in the firing rates of STN neurons recorded from R6/2 mice compared to WT mice. In addition, the discharge patterns of STN neurons in R6/2 mice were significantly less regular compared to WT mice. Hence, the highly conserved fast spiking, tonic discharge during desynchronized ECoG conditions in STN neurons (Bevan *et al.* 2002) is disrupted as a function of the mHtt protein. The importance of continuous persistent discharge by STN neurons is exemplified by the fact that experimental or pathological disruption of repetitive firing in the STN is associated with hyperkinetic symptoms (Crossman, 1989; Hamada & DeLong, 1992) similar to that seen in HD. There are several mechanisms that could drive the abnormally patterned discharge of STN neurons during desynchronized states that will need to be addressed in future studies. As striatal degeneration is a cardinal pathology in HD, disinhibition of neurons in the globus pallidus external segment (GPe) could result in an augmented GABAergic tone in the STN in HD. The GPe exerts powerful GABAergic control over the STN (Smith *et al.* 1990; Bevan *et al.* 2007) and neuronal network simulations have indicated that irregular activity can arise in the STN when GPe inhibition is strong and striatal inhibition is weak (Terman *et al.* 2002). In addition, we

cannot rule out the possibility that intrinsic membrane properties of STN neurons are altered as function of the expression of the mHtt protein in R6/2 mice.

The present results show profound reductions in the entrainment of STN activity to coordinated cortical inputs, as well as overall reductions in the spontaneous firing rates of STN neurons in HD mice. As the STN comprises the principal excitatory glutamatergic input to the basal ganglia output nuclei, the dramatic disruption in the activity of STN neurons could lead to errors in the fidelity of information transmission within cortico-basal ganglia loops and result in disordered motor function in HD.

# References

Amzica F & Steriade M (1998). Electrophysiological correlates of sleep delta waves. *Electroencephalogr Clin Neurophysiol* **107**, 69–83.

Barnes TD, Kubota Y, Hu D, Jin DZ & Graybiel AM (2005). Activity of striatal neurons reflects dynamic encoding and recoding of procedural memories. *Nature* **437**, 1158–1161.

Baunez C & Robbins TW (1997). Bilateral lesions of the subthalamic nucleus induce multiple deficits in an attentional task in rats. *Eur J Neurosci* **9**, 2086–2099.

Bevan MD, Francis CM & Bolam JP (1995). The glutamate-enriched cortical and thalamic input to neurons in the subthalamic nucleus of the rat: convergence with GABA-positive terminals. *J Comp Neurol* **361**, 491–511.

Bevan MD, Hallworth NE & Baufreton J (2007). GABAergic control of the subthalamic nucleus. *Prog Brain Res* **160**, 173–188.

Bevan MD, Magill PJ, Terman D, Bolam JP & Wilson CJ (2002). Move to the rhythm: oscillations in the subthalamic nucleus–external globus pallidus network. *Trends Neurosci* **25**, 525–531.

Bevan MD & Wilson CJ (1999). Mechanisms underlying spontaneous oscillation and rhythmic firing in rat subthalamic neurons. *J Neurosci* **19**, 7617–7628.

Bokil H, Andrews P, Kulkarni JE, Mehta S & Mitra PP (2010). Chronux: a platform for analyzing neural signals. *J Neurosci Methods* **192**, 146–151.

Brenner RP (1985). The electroencephalogram in altered states of consciousness. *Neurol Clin* **3**, 615–631.

Brown P (2003). Oscillatory nature of human basal ganglia activity: relationship to the pathophysiology of Parkinson's disease. *Mov Disord* **18**, 357–363.

Callahan JW & Abercrombie, ED (2011). *In vivo* dopamine efflux is decreased in striatum of both fragment (R6/2) and full-length (YAC128) transgenic mouse models of Huntington's disease. *Front Syst Neurosci.* **5**, 61.

Carpenter MB, Whittier JR & Mettler FA (1950). Analysis of choreoid hyperkinesia in the Rhesus monkey; surgical and pharmacological analysis of hyperkinesia resulting from lesions in the subthalamic nucleus of Luys. *J Comp Neurol* **92**, 293–331.

Cepeda C, Hurst RS, Calvert CR, Hernández-Echeagaray E, Nguyen OK, Jocoy E, Christian LJ, Ariano MA & Levine MS (2003). Transient and progressive electrophysiological alterations in the corticostriatal pathway in a mouse model of Huntington's disease. *J Neurosci* 23, 961–969.

Cepeda C, Wu N, Andre VM, Cummings DM & Levine MS (2007). The corticostriatal pathway in Huntington's disease. *Prog Neurobiol* 81, 253–271.

Crossman AR (1989). Neural mechanisms in disorders of movement. *Comp Biochem Physiol A Comp Physiol* 93, 141–149.

Crupi D, Ghilardi MF, Mosiello C, Di Rocco A, Quartarone A & Battaglia F (2008). Cortical and brainstem LTP-like plasticity in Huntington's disease. *Brain Res Bull* 75, 107–114.

Dallerac GM, Vatsavayai SC, Cummings DM, Milnerwood AJ, Peddie CJ, Evans KA, Walters SW, Rezaie P, Hirst MC & Murphy KP (2011). Impaired long-term potentiation in the prefrontal cortex of Huntington's disease mouse models: rescue by D1 dopamine receptor activation. *Neurodegener Dis* 8, 230–239.

DiFiglia M, Sapp E, Chase KO, Davies SW, Bates GP, Vonsattel JP & Aronin N (1997). Aggregation of huntingtin in neuronal intranuclear inclusions and dystrophic neurites in brain. *Science* 277, 1990–1993.

Ferron JF, Kroeger D, Chever O & Amzica F (2009). Cortical inhibition during burst suppression induced with isoflurane anesthesia. *J Neurosci* 29, 9850–9860.

Fisher SP, Black SW, Schwartz MD, Wilk AJ, Chen TM, Lincoln WU, Liu HW, Kilduff TS & Morairty SR (2013). Longitudinal analysis of the electroencephalogram and sleep phenotype in the R6/2 mouse model of Huntington's disease. *Brain* 136, 2159–2172.

Franklin KBJ & Paxinos G (2008). The Mouse Brain in Stereotaxic Coordinates. Elsevier Academic, Amsterdam.

Fujimoto K & Kita H (1993). Response characteristics of subthalamic neurons to the stimulation of the sensorimotor cortex in the rat. *Brain Res* 609, 185–192.

Hamada I & DeLong MR (1992). Excitotoxic acid lesions of the primate subthalamic nucleus result in transient dyskinesias of the contralateral limbs. *J Neurophysiol* 68, 1850–1858.

Hassani OK, Francois C, Yelnik J & Feger J (1997). Evidence for a dopaminergic innervation of the subthalamic nucleus in the rat. *Brain Res* 749, 88–94.

Hickey MA, Reynolds GP & Morton AJ (2002). The role of dopamine in motor symptoms in the R6/2 transgenic mouse model of Huntington's disease. *J Neurochem* 81, 46–59.

Hong SL, Cossyleon D, Hussain WA, Walker LJ, Barton SJ & Rebec GV (2012). Dysfunctional behavioral modulation of corticostriatal communication in the R6/2 mouse model of Huntington's disease. *PLoS One* 7, e47026.

Hughes S & Crunelli V (2013). UP states rise from the depths. *Nat Neurosci* 16, 115–117.

Jackson A & Crossman AR (1983). Nucleus tegmenti pedunculopontinus: efferent connections with special reference to the basal ganglia, studied in the rat by anterograde and retrograde transport of horseradish peroxidase. *Neuroscience* 10, 725–765.

Johnson MA, Rajan V, Miller CE & Wightman RM (2006). Dopamine release is severely compromised in the R6/2 mouse model of Huntington's disease. *J Neurochem* 97, 737–746.

Kaneoke Y & Vitek JL (1996). Burst and oscillation as disparate neuronal properties. *J Neurosci Methods* 68, 211–223.

Kantor S, Szabo L, Varga J, Cuesta M & Morton AJ (2013). Progressive sleep and electroencephalogram changes in mice carrying the Huntington's disease mutation. *Brain* 136, 2147–2158.

Klapstein GJ, Fisher RS, Zanjani H, Cepeda C, Jokel ES, Chesselet MF & Levine MS (2001). Electrophysiological and morphological changes in striatal spiny neurons in R6/2 Huntington's disease transgenic mice. *J Neurophysiol* 86, 2667–2677.

Kuki T, Ohshiro T, Ito S, Ji ZG, Fukazawa Y, Matsuzaka Y, Yawo H & Mushiake H (2013). Frequency-dependent entrainment of neocortical slow oscillation to repeated optogenetic stimulation in the anesthetized rat. *Neurosci Res* 75, 35–45.

Kung VW, Hassam R, Morton AJ & Jones S (2007). Dopamine-dependent long term potentiation in the dorsal striatum is reduced in the R6/2 mouse model of Huntington's disease. *Neuroscience* 146, 1571–1580.

Laforet GA, Sapp E, Chase K, McIntyre C, Boyce FM, Campbell M, Cadigan BA, Warzecki L, Tagle DA, Reddy PH *et al.* (2001). Changes in cortical and striatal neurons predict behavioral and electrophysiological abnormalities in a transgenic murine model of Huntington's disease. *J Neurosci* 21, 9112–9123.

Lavoie B & Parent A (1990). Immunohistochemical study of the serotoninergic innervation of the basal ganglia in the squirrel monkey. *J Comp Neurol* 299, 1–16.

Litvak V, Jha A, Eusebio A, Oostenveld R, Foltynie T, Limousin P, Zrinzo L, Hariz MI, Friston K & Brown P (2011). Resting oscillatory cortico-subthalamic connectivity in patients with Parkinson's disease. *Brain* 134, 359–374.

Magill PJ, Bolam JP & Bevan MD (2000). Relationship of activity in the subthalamic nucleus–globus pallidus network to cortical electroencephalogram. *J Neurosci* 20, 820–833.

Magill PJ, Bolam JP & Bevan MD (2001). Dopamine regulates the impact of the cerebral cortex on the subthalamic nucleus–globus pallidus network. *Neuroscience* 106, 313–330.

Magill PJ, Sharott A, Bevan MD, Brown P & Bolam JP (2004). Synchronous unit activity and local field potentials evoked in the subthalamic nucleus by cortical stimulation. *J Neurophysiol* 92, 700–714.

Mallet N, Pogosyan A, Sharott A, Csicsvari J, Bolam JP, Brown P & Magill PJ (2008). Disrupted dopamine transmission and the emergence of exaggerated beta oscillations in subthalamic nucleus and cerebral cortex. *J Neurosci* 28, 4795–4806.

Mangiarini L, Sathasivam K, Seller M, Cozens B, Harper A, Hetherington C, Lawton M, Trottier Y, Lehrach H, Davies SW & Bates GP (1996). Exon 1 of the HD gene with an expanded CAG repeat is sufficient to cause a progressive neurological phenotype in transgenic mice. *Cell* 87, 493–506.

Maurice N, Deniau JM, Glowinski J & Thierry AM (1998). Relationships between the prefrontal cortex and the basal ganglia in the rat: physiology of the corticosubthalamic circuits. *J Neurosci* **18**, 9539–9546.

Miller BR, Walker AG, Barton SJ & Rebec GV (2011). Dysregulated neuronal activity patterns implicate corticostriatal circuit dysfunction in multiple rodent models of Huntington's disease. *Front Syst Neurosci* **5**, 26.

Mink JW (1996). The basal ganglia: focused selection and inhibition of competing motor programs. *Prog Neurobiol* **50**, 381–425.

Mochel F, Durant B, Durr A & Schiffmann R (2011). Altered dopamine and serotonin metabolism in motorically asymptomatic R6/2 mice. *PLoS One* **6**, e18336.

Morton AJ (2013). Circadian and sleep disorder in Huntington's disease. *Exp Neurol* **243**, 34–44.

Nambu A, Tokuno H, Hamada I, Kita H, Imanishi M, Akazawa T, Ikeuchi Y & Hasegawa N (2000). Excitatory cortical inputs to pallidal neurons via the subthalamic nucleus in the monkey. *J Neurophysiol* **84**, 289–300.

Nambu A, Tokuno H & Takada M (2002). Functional significance of the cortico-subthalamo-pallidal 'hyperdirect' pathway. *Neurosci Res* **43**, 111–117.

Pallier PN, Drew CJ & Morton AJ (2009). The detection and measurement of locomotor deficits in a transgenic mouse model of Huntington's disease are task- and protocol-dependent: influence of non-motor factors on locomotor function. *Brain Res Bull* **78**, 347–355.

Raymond LA, Andre VM, Cepeda C, Gladding CM, Milnerwood AJ & Levine MS (2011). Pathophysiology of Huntington's disease: time-dependent alterations in synaptic and receptor function. *Neuroscience* **198**, 252–273.

Rosas HD, Liu AK, Hersch S, Glessner M, Ferrante RJ, Salat DH, van der Kouwe A, Jenkins BG, Dale AM & Fischl B (2002). Regional and progressive thinning of the cortical ribbon in Huntington's disease. *Neurology* **58**, 695–701.

Sapp E, Penney J, Young A, Aronin N, Vonsattel JP & DiFiglia M (1999). Axonal transport of N-terminal huntingtin suggests early pathology of corticostriatal projections in Huntington disease. *J Neuropathol Exp Neurol* **58**, 165–173.

Smith Y, Bolam JP & VonKrosigk M (1990). Topographical and synaptic organization of the GABA-containing pallidosubthalamic projection in the rat. *Eur J Neurosci* **2**, 500–511.

Sotrel A, Williams RS, Kaufmann WE & Myers RH (1993). Evidence for neuronal degeneration and dendritic plasticity in cortical pyramidal neurons of Huntington's disease: a quantitative Golgi study. *Neurology* **43**, 2088–2096

Stack EC, Kubilus JK, Smith K, Cormier K, Del Signore SJ, Guelin E, Ryu H, Hersch SM & Ferrante RJ (2005). Chronology of behavioral symptoms and neuropathological sequela in R6/2 Huntington's disease transgenic mice. *J Comp Neurol* **490**, 354–370.

Stern EA (2011). Functional Changes in Neocortical Activity in Huntington's Disease Model Mice: An in vivo Intracellular Study. *Front Syst Neurosci* **5**, 47.

Steriade M (2001). Impact of network activities on neuronal properties in corticothalamic systems. *J Neurophysiol* **86**, 1–39.

Steriade M, Nunez A & Amzica F (1993). A novel slow (<1 Hz) oscillation of neocortical neurons *in vivo*: depolarizing and hyperpolarizing components. *J Neurosci* **13**, 3252–3265.

Terman D, Rubin JE, Yew AC & Wilson CJ (2002). Activity patterns in a model for the subthalamopallidal network of the basal ganglia. *J Neurosci* **22**, 2963–2976.

Turmaine M, Raza A, Mahal A, Mangiarini L, Bates GP & Davies SW (2000). Nonapoptotic neurodegeneration in a transgenic mouse model of Huntington's disease. *Proc Natl Acad Sci U S A* **97**, 8093–8097.

Vonsattel JP & DiFiglia M (1998). Huntington disease. *J Neuropathol Exp Neurol* **57**, 369–384.

Walker AG, Miller BR, Fritsch JN, Barton SJ & Rebec GV (2008). Altered information processing in the prefrontal cortex of Huntington's disease mouse models. *J Neurosci* **28**, 8973–8982.

Whelan G & Flecknell PA (1992). The assessment of depth of anaesthesia in animals and man. *Lab Anim* **26**, 153–162.

Whittier JR & Mettler FA (1949). Studies on the subthalamus of the rhesus monkey; hyperkinesia and other physiologic effects of subthalamic lesions; with special reference to the subthalamic nucleus of Luys. *J Comp Neurol* **90**, 319–372.

## Additional information

### Competing interests

The authors declare no competing interests.

### Author contributions

J.W.C. performed the research, analysed the data and wrote and revised the manuscript; E.D.A. designed the experiments and wrote and revised the manuscript.